AGU PUBLICATIONS

Geophysical Research Letters

RESEARCH LETTER
10.1002/2013GL058888

Key Points:
- Large improvement in oxygen field representation in an eddy resolving model
- Major sensitivity of OMZs extension to the equatorial current system strength
- Asymmetric response of oxygen supply and consumption to circulation intensity

Supporting Information:
- Readme
- Figure S1
- Figure S2
- Figure S3

Correspondence to:
O. Duteil,
oduteil@geomar.de

Citation:
Duteil, O., F. U. Schwarzkopf, C. W. Böning, and A. Oschlies (2014), Major role of the equatorial current system in setting oxygen levels in the eastern tropical Atlantic Ocean: A high-resolution model study, *Geophys. Res. Lett.*, *41*, 2033–2040, doi:10.1002/2013GL058888.

Received 3 DEC 2013
Accepted 17 JAN 2014
Accepted article online 20 JAN 2014
Published online 17 MAR 2014

Major role of the equatorial current system in setting oxygen levels in the eastern tropical Atlantic Ocean: A high-resolution model study

Olaf Duteil[1], Franziska U. Schwarzkopf[1], Claus W. Böning[1], and Andreas Oschlies[1]

[1]GEOMAR Helmholtz Centre for Ocean Research Kiel, Kiel, Germany

Abstract Understanding the causes of the observed expansion of tropical ocean's oxygen minimum zones (OMZs) is hampered by large biases in the representation of oxygen distribution in climate models, pointing to incorrectly represented mechanisms. Here we assess the oxygen budget in a global biogeochemical circulation model, focusing on the Atlantic Ocean. While a coarse (0.5°) configuration displays the common bias of too large and too intense OMZs, the oxygen concentration in an eddying (0.1°) configuration is higher and closer to observations. This improvement is traced to a stronger oxygen supply by a more realistic representation of the equatorial and off-equatorial undercurrents, outweighing the concurrent increase in oxygen consumption associated with the stronger nutrient supply. The sensitivity of the eastern tropical Atlantic oxygen budget to the equatorial current intensity suggests that temporal changes in the eastward oxygen transport from the well-oxygenated western boundary region might partly explain variations in the OMZs.

1. Introduction

The oxygen distribution in the ocean is the result of complex interactions between biogeochemistry and circulation. Remineralization of sinking organic material consumes oxygen in the ocean interior, while physical transport of waters ventilated at the ocean surface tends to resupply oxygen by advective or diffusive processes. Intense oxygen minimum zones (OMZs) are commonly observed at intermediate depth along the eastern boundaries of the tropical Atlantic and Pacific Oceans [e.g., *Stramma et al.*, 2008], which are characterized by both high organic matter export and weak interior ventilation. OMZs closely coincide with the so-called "shadow zones" [*Luyten et al.*, 1983], characterized by a sluggish cyclonic circulation.

Understanding the causes of the observed OMZs' expansion [*Stramma et al.*, 2008] is hampered by large biases in climate models. Simulated oxygen concentrations in the eastern equatorial and tropical regions are generally underestimated [*Oschlies et al.*, 2008; *Deutsch et al.*, 2011; *Duteil and Oschlies*, 2011; *Gnanadesikan et al.*, 2012; *Stramma et al.*, 2012; *Cocco et al.*, 2013], in particular, in the Atlantic Ocean. An unrealistic representation of the circulation, and more specifically of the equatorial current system, might be responsible for the discrepancy between models and observations [*Dietze and Loeptien*, 2013]. In the tropical Atlantic Ocean, the oxygen-rich waters of the North Brazil Current (NBC) are connected with the eastern part of the basin principally via the eastward flowing Equatorial Undercurrent (EUC) [*Stramma and Schott*, 1999]. The EUC is flanked by its eastward flowing southern and northern branches (SEUC and NEUC) around 5°N and 5°S. A simple conceptual model suggested that a variation in the strength of extraequatorial jets impacts the mean equatorial oxygen distribution [*Brandt et al.*, 2010].

Another potential source of bias arises from the simplification of biogeochemical processes by the models. High-productivity regions are located on the eastern side of the Atlantic basin due to the presence of upwelling systems, which carry nutrients from the ocean interior toward the surface. The interior oxygen concentration is sensitive to the rate of export, decay, and remineralization of organic matter, which are often parameterized in a simple way [e.g., *Kriest et al.*, 2010]. Identifying to what extent the representation of circulation or biogeochemistry is deficient in existing models is not an easy task, as the biogeochemical parameters are often "tuned" in order to achieve a realistic representation of nutrient fields and thereby may compensate possible deficiencies in the simulated ocean circulation [*Duteil et al.*, 2012].

Here we assess the sensitivity of simulated oxygen concentrations to a refinement of the horizontal grid resolution of a coupled circulation biogeochemistry model, with the biogeochemical model staying unchanged. A change in resolution impacts the circulation strength, and in particular the equatorial currents. Faster (slower) currents, on the one hand, lead to higher (lower) ventilation rates and transport of tracers, such as oxygen. On the other hand, a change in nutrient transport might trigger changes in biological productivity, with consequences for oxygen consumption at depth. Our analysis aims at differentiating between changes in oxygen supply and oxygen consumption.

2. Model Experiments

The ocean model builds on the NEMO (Nucleus for European Modelling of the Ocean) v3.1 code [*Madec*, 2008]. Two configurations are used in this study, both of them including 46 vertical levels, with increasing thickness from 6 m at the surface to 250 m at depth. The configurations differ in their horizontal resolution:

1. ORCA05: the global ocean model has a nominal resolution in latitude and longitude of 0.5° by 0.5° cos φ (where φ is the latitude). Effects of unresolved mesoscale eddies are parameterized following *Gent and McWilliams* [1990].
2. TRATL01: a 0.1° resolution two ways AGRIF (Adaptive Grid Refinement In Fortran) nest [*Debreu et al*., 2008] nest has been embedded between 30°N and 30°S in the Atlantic Ocean into a global ORCA05 grid. Since the model is eddying in the nested region the *Gent and McWilliams*' [1990] parameterization is not used there.

Both configurations are forced by the same interannually varying atmospheric data given by the Coordinated Ocean-Ice Reference Experiments (CORE) v2 reanalysis products over the period 1948–2007 [*Large and Yeager*, 2009], starting from the same initial conditions. The initial fields for the physical variables are given by the final state of a 60 year integration of TRATL01 (using 1948–2007 interannual forcing and following an initial 80 year climatological spin-up at coarse resolution). The interpretation of differences in the ventilation of thermocline waters in the two models is aided by an ideal age tracer, which records the time since the last contact of a water parcel with the atmosphere during the spin-up of the circulation.

The ocean circulation model is coupled with a simple biogeochemical model, based on six prognostic variables. The inorganic variables include dissolved oxygen (O_2) and phosphate (PO_4). They are linked through exchanges with the biological variables (phytoplankton, zooplankton, particulate, and dissolved organic matter) by a constant Redfield stoichiometry C:N:P:O_2 of 122:16:1:−170. The PO_4 and O_2 fields are initialized from the World Ocean Atlas (WOA) [*Garcia et al*., 2010]. The air-sea flux of oxygen is formulated according to the Ocean Carbon-Cycle Model Intercomparison Project (OCMIP) protocol [*Najjar et al*., 2007]. This nutrient-phytoplankton-zooplankton-detritus (NPZD) biogeochemical model was first used in a global model by *Schmittner et al*. [2005] and is employed here with the parameter set obtained by *Kriest et al*. [2010] by calibrating a coarse-resolution global model configuration against the observed global pattern of nutrients and oxygen. In this experiment, the phytoplankton growth (maximal growth rate of 0.6 d^{-1} at 0°C) is set by the most limiting resource, whether nutrients or light. The linear phytoplankton loss term (mortality) is 0.01 d^{-1}. The quadratic loss term is 0.03125 mmol P m^{-3} d^{-1} and can be considered as a parameterization of various loss processes (e.g., aggregation of phytoplankton cells or viral lysis). Particle sinking speed increases linearly with depth, with values ranging from 5 m d^{-1} below the mixed layer to 280 m d^{-1} in the deepest layer. The detritus remineralization rate is constant and equal to 0.05 d^{-1}.

The model years analyzed hereafter are 1998–2007 averages, with TRATL01 outputs regridded on the ORCA05 mesh to facilitate intercomparison of the two configurations.

3. Oxygen Concentrations in WOA, ORCA05, and TRATL01

Observed WOA oxygen concentrations are characterized by a pronounced minimum in the eastern part of the tropical Atlantic (Figure 1a). The lowest concentrations, of about 30 mmol m^{-3} at about 400 m depth (Figure 1b), are observed in the Atlantic South East Tropical Upwelling System (ASETUS), which comprises the Angola dome and the Angola and Benguela upwelling (0°E–coast, 5°S–25°S). Minimum concentrations are somewhat higher (50 mmol m^{-3}) in the Atlantic North East Tropical Upwelling System (ANETUS), which comprises the Guinea Dome and the Mauritanian and Senegal upwelling regions. The equatorial band

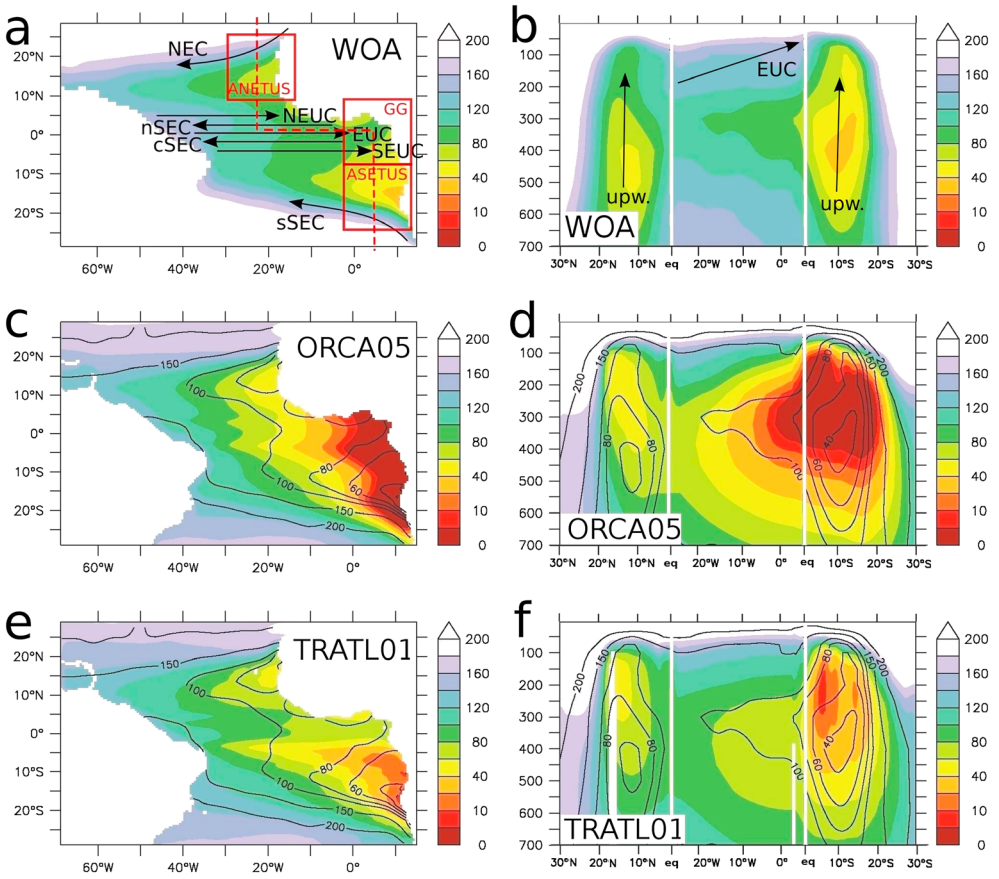

Figure 1. (a) Oxygen concentration (mmol m^{-3}) in WOA in the 200 m–400 m depth layer and (b) along the section marked with red dashes on Figure 1a. The main currents are schematically represented. Oxygen concentration for the same depth layer and section (c and d) in ORCA05 and (e and f) in TRATL01. The model fields are 1998–2007 averages. WOA data are represented as contours. The ANETUS (Atlantic North East Tropical Upwelling System), ASETUS (Atlantic South East Tropical Upwelling System), and GG (Guinea Gulf) regions are depicted by red boxes. The evolution of the interior oxygen concentration in the ANETUS, GG, and ASETUS regions from 1948 to 2007 is presented in Figure S1.

(5°N–5°S) is comparatively better ventilated. Minimum oxygen concentrations of 80 mmol.m^{-3} are observed at 300 m depth in the Gulf of Guinea (GG: 0°E–coast, 5°S–5°N) below the EUC.

The ORCA05 experiment (Figure 1c) results in large and unrealistic suboxic regions (oxygen lower than 5 mmol m^{-3}), extending from the GG to the ASETUS region, between 200 m to 400 m depth (Figure 1d). The oxygen minimum is located around 300 m depth, somewhat shallower than in the observations. This discrepancy in the vertical profile might reflect errors in the remineralization profile of the exported organic matter. Simulated oxygen concentrations are higher and closer to the observations in the ANETUS region. Compared to ORCA05, the oxygen concentration in the eastern part of the basin is significantly higher and more realistic in TRATL01 (Figures 1e and 1f). In agreement with the observations, low oxygen (<40 mmol m^{-3}) values are restricted to the ASETUS region. In the GG region the differences between the two model configurations are most striking: minimum oxygen concentrations in TRATL01 are of the order of 60 mmol m^{-3}, closer to the 80 mmol m^{-3} observed in WOA, whereas this region is completely depleted in oxygen in ORCA05. Simulated oxygen concentrations in the ANETUS region are only slightly higher by about 10 mmol m^{-3} in TRATL01, but again more realistic than in ORCA05. The western part of the Atlantic and the subtropical gyres exhibit comparable oxygen values in both experiments.

4. Mechanisms Controlling the Oxygen Concentration

4.1. Circulation

In the OMZ depth layer, between 200 m and 400 m, the mean current speed in the tropical region reflects both the extension and strength of the upper and the deeper thermocline currents. In ORCA05 (Figure 2a),

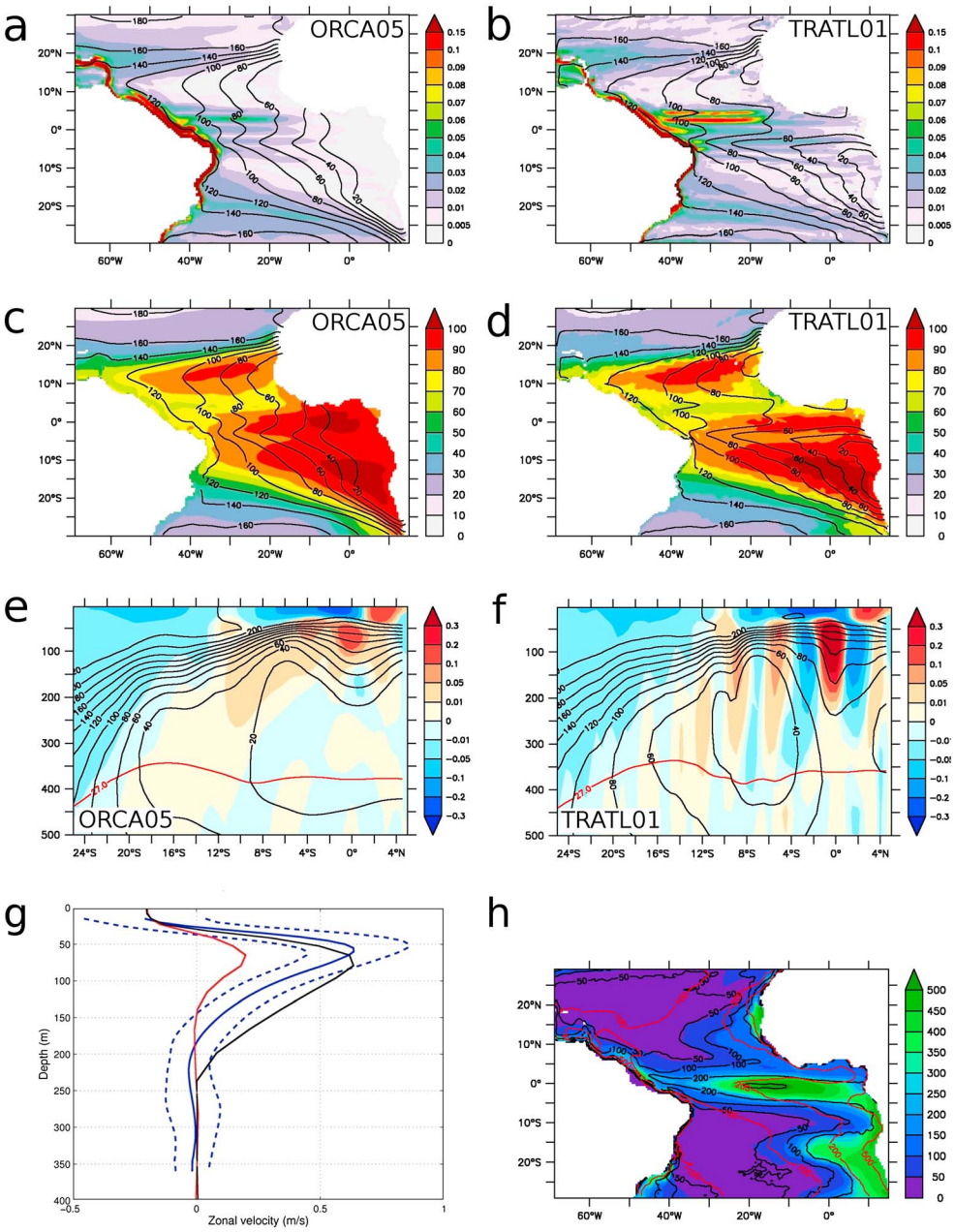

Figure 2. Absolute value of the mean current velocity (m s^{-1}) in the 200 m–400 m depth layer (a) in ORCA05 and (b) in TRATL01. Ideal age in the 200 m–400 m depth layer (years) (c) in ORCA05 and (d) in TRATL01. Contours denote oxygen concentrations (mmol m^{-3}) at 200 m–400 m depth in all panels. Meridional section of the mean zonal velocity (m s^{-1}) at 0°E (e) in ORCA05 and (f) in TRATL01. Mean oxygen concentrations (mmol m^{-3}) are traced in black, the 27.0 density isoline in red. (g) Mean zonal velocity (m s^{-1}) at 0°N/0°E for ORCA05 (red), TRATL01 (black), and in observations (PIRATA mooring) [*Johns et al.*, 2012] (blue). (h) TRATL01 net primary production (NPP) (mgC $m^{-2}yr^{-1}$). ORCA05 NPP is traced in black contours; observed NPP is traced in red. All the model fields, except the ideal age, are 1998–2007 averages.

the equatorial current system is poorly developed. The mean currents in the 200 m–400 m depth range are sluggish east of 10°W. In TRATL01 (Figure 2b), the lower edge of the EUC, flowing along the equator, and the SEUC, flowing between 5°S and 10°S can be identified. These jets cross the entire Atlantic and flow eastward from the oxygen-rich NBC to the eastern part of the Guinea Gulf. The NECC/NEUC flow eastward around 5°N. The velocity of the westward flowing North and South Equatorial Currents, forming the equatorward margin of the subtropical gyres, is comparable in both experiments.

The circulation pattern maps onto the simulated ideal age distribution. In TRATL01 (Figure 2d), the average age in the 200 m–400 m layer along the eastern side of the equatorial region is lower (70 to 100 years) than in ORCA05 (Figure 2c) (greater than 100 years). The northern and southern shadow zones, associated with the ANETUS and ASETUS, are characterized by waters older than 90 years in both experiments. The ventilation by the EUC, NEUC, and SEUC leads to the formation of tongues of younger water, a few degrees north of the equator and around 5°S, especially in TRATL01. The water is significantly younger in TRATL01 than in ORCA05 in the GG region. In the thermocline of the subtropical gyres, waters are relatively young and of similar age in both experiments.

To better assess the role of oxygen transport, the equatorial and tropical zonal current structure is inspected. The most prominent current in the upper thermocline is the eastward EUC, flanked by the westward central and northern South Equatorial Currents. TRATL01 differs from ORCA05 primarily by a more pronounced eastward penetration of the EUC, as at 0°E the maximum zonal velocity is 0.55 m s^{-1} in TRATL01 (Figure 2f) compared to only 0.1 m s^{-1} in ORCA05 (Figure 2e). The mean zonal velocity profile at this location agrees well with the observed profile (Figure 2g) obtained from moored current meter measurements [*Johns et al.*, 2012]. South of the EUC the SEUC flows eastward between 5°S and 10°S. At 0°E, the SEUC is very sluggish and not clearly isolated from the mean flow field in ORCA05 (Figure 2a), whereas the two observed SEUC branches are clearly identified in TRATL01 (Figure 2b). South of these branches (12°S to 15°S), two eastward flowing jets ventilate the interior ocean at 200 m to 300 m depth. The strong difference in the representation of the equatorial current system between the two models is reflected in the simulated oxygen concentration (Figure 1).

4.2. Biological Production

Oxygen is consumed in the deep ocean by the remineralization of organic matter, which mainly originates from biological production in the euphotic layer. Net primary production (NPP) consequently constraints oxygen consumption. Synoptic observational estimates of NPP can be obtained from remote sensing data by algorithms such as the vertically generalized production model (VGPM) [*Behrenfeld and Falkowski*, 1997]. The modeled NPP pattern is similar in ORCA05 and TRATL01 and in broad agreement with the satellite-derived NPP pattern computed by the VGPM (Figures 2h and S2a–S2d in the supporting information) despite the simplicity of the NPZD model (constant C:N:P stoichiometry, constant remineralization rates, neglect of denitrification/anammox, and interactions with the sediment). The modeled NPP values, however, tend to be lower (production in the gyres below 50 gC m^{-2} yr^{-1} and between 400 and 450 gC m^{-2} yr^{-1} in the upwelling regions) except for the equatorial region where the models exhibit a too high productivity. The integrated NPP over the basin is lower in ORCA05 (4.36 GtC yr^{-1}) and TRATL01 (4.43 GtC yr^{-1}) compared to the observations (6.98 GtC yr^{-1}). Simulated NPP values in ORCA05 and TRATL01 are similar because phosphate is not the immediate factor limiting phytoplankton growth in the eastern high-productivity regions, consistent with observational and experimental evidence [*Moore et al.*, 2013]. The phytoplankton growth is primarily limited by light (see Figures S2e and S2f) in both model configurations, making the NPP relatively insensitive to an extra input of nutrients due to a change in circulation.

4.3. Integrated Budget

The changes in oxygen concentration between the two model solutions are a consequence of either changes in the supply of oxygen by the flow field or the consumption of oxygen by biological processes. Consider the balance between supply processes (S) and biological oxygen consumption (C) in the OMZ layers (200 m–400 m): any difference between the two processes is reflected in a temporal trend of the oxygen content, i.e., $dO_2/dt = S - C$.

We first diagnose the mean trend dO_2/dt of the oxygen inventory in the Atlantic basin during the 60 year simulation periods in ORCA05 and TRATL01. These temporal trends are negative (see Figures 3a, 3b, and S1), i.e., both simulations lose oxygen and adjust to concentrations below the values given by the WOA, used for initialization. As the initial oxygen concentration is not in equilibrium, the mean temporal oxygen trend during the first decades of the integration reflects primarily the models' adjustment to the circulation and biogeochemistry. The impact of interannual variability on the mean trend is comparatively small and is neglected in this study. We focus on the adjustment process.

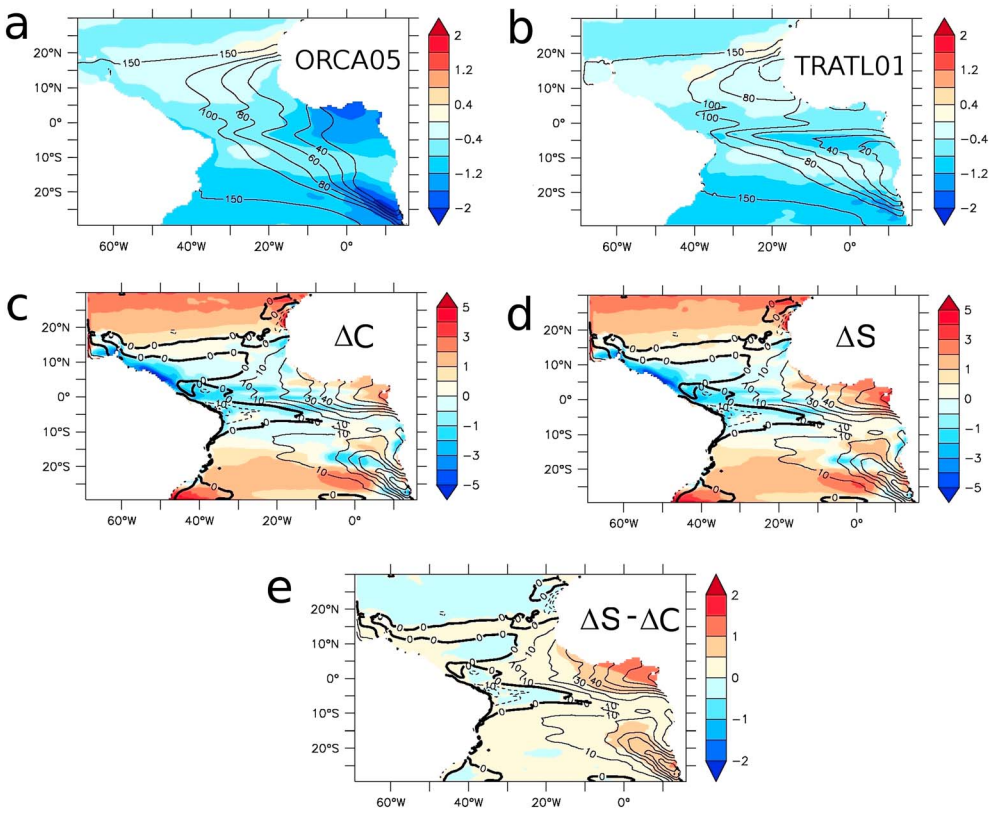

Figure 3. Mean oxygen trend dO_2/dt (mmol m^{-3} yr^{-1}) during the integration period 1948–2007 of (a) ORCA05 and (b) TRATL01. The final (average 1998–2007) oxygen concentration (mmol m^{-3}) is traced in contours. (c) Difference ΔC (mmol m^{-3} yr^{-1}) between the biological consumption term C in TRATL01 and ORCA05 (average 1948–2007). (d) Difference ΔS (mmol m^{-3} yr^{-1}) between the circulation supply term S in TRATL01 and ORCA05 (average 1948–2007). (e) Regions where the difference in supply exceeds the difference in consumption: $\Delta T = \Delta S - \Delta C$. The difference in final (average 1998–2007) oxygen concentration (mmol m^{-3}) between TRATL01 and ORCA05 is shown in contour in Figures 3c–3e. All the fields are averages for the depth layer 200 m–400 m.

The negative trends are substantially reduced in TRATL01, especially in the GG and ASETUS region, suggesting that the circulation and biogeochemistry are closer to reality in TRATL01 compared to ORCA05. ORCA05 loses up to 2 mmol m^{-3} yr^{-1} in both regions, whereas the trend is diminished in TRATL01 to less than 0.6 mmol m^{-3} yr^{-1} in the GG and less than 1.2 mmol m^{-3} yr^{-1} in the ASETUS.

In principle, changes in the structure and/or strength of the current system should affect both the supply of oxygen to these regions (by the oxygen flux from the western tropical Atlantic) and the consumption (by changes in the nutrient supply and associated changes in biological productivity) (Figure S3). Inspecting the changes in the individual consumption and supply rates between ORCA05 and TRATL01 reveals that the intensified equatorial currents in the latter simulation affect the oxygen supply (Figure 3d) more strongly than the consumption (Figure 3c). For instance, in the GG, supply increases by up to 50% in TRATL01 compared to ORCA05, while the concomitant increase in consumption is only 20%. As a consequence, the difference in supply exceeds the difference in consumption (Figure 3e), resulting in a significant increase of oxygen concentrations in TRATL01.

5. Summary and Conclusion

The oxygen distribution in the interior ocean was assessed in two hindcast experiments with a global coupled physical-biogeochemical model, which differed only in their spatial resolution. Both coarse (0.5°) and eddying (0.1°) model configurations (ORCA05 and TRATL01) were integrated under realistic forcing conditions over the period 1948–2007 and initialized from climatological (WOA) conditions for oxygen and phosphate. The analysis focused on the oxygen adjustment over the simulation period and the distributions in the last decade (1998–2007) of both simulations.

While the 0.5° model exhibits a strong negative oxygen trend especially in the GG and ASETUS regions, leading to too intensive OMZs, the trends are much weaker and the averaged oxygen concentrations much more realistic in the 0.1° case, both in the equatorial region (GG), and in the northern and southern shadow zones (ANETUS and ASETUS). The differences in the simulated oxygen concentration in the eastern tropical Atlantic can be understood as an effect of an enhanced oxygen supply by the more intense equatorial current system in the 0.1° case. The GG region is ventilated mainly by the EUC, which especially in its eastern portion is much stronger, more structured and more realistic in the high-resolution case. The ASETUS region is ventilated by the off-equatorial current (SEUC) along its northern flank, and by the sSEC at its southern boundary. Since the sSEC has similar characteristics in both experiments, the strength of the SEUC appears to be a critical factor in governing the oxygen concentrations in this region. The resolution-dependent intensification of the zonal undercurrents is mostly confined to the eastern part of the basin, i.e., to the east of about 10° W. Accordingly, the impact of resolution is most pronounced in the GG and ASETUS, and comparatively weak in the ANETUS.

Despite clear improvement in the high-resolution model, a tendency toward too low oxygen concentrations in the eastern tropical Atlantic compared to the conditions given by the WOA remains, suggesting that some processes are still not correctly captured even in the high-resolution model. Possible flaws include a too weak transport by the eastward flowing Southern and Northern Intermediate Counter Currents, which are suggested to ventilate the eastern tropical regions [*Brandt et al*., 2012; *Getzlaff and Dietze*, 2013]. Deficits may also be related to the representation of biogeochemical processes. Oxygen, for instance, is very sensitive to changes in the remineralization length scale and in simulated primary production [*Kriest et al*., 2012]. The behavior of organisms, such as zooplankton migrating patterns, also influences the oxygen consumption [*Bianchi et al*., 2013]. Regional variations in phytoplankton properties, for example, in C:N:P stoichiometry [*Martiny et al*., 2013], have not been taken into account here.

A more fundamental aspect of the eastern tropical oxygen budgets highlighted by the present experiments is the different sensitivity of the oxygen supply and consumption processes to changes in the strength of the equatorial current system. Since relatively small perturbations of the balance between supply and consumption can lead to significant temporal trends in the oxygen content of the OMZs, the present results suggests that trends or low-frequency variations in the equatorial currents [e.g., *Brandt et al*., 2010; *Jouanno et al*., 2011; *Goes et al*., 2013] could represent a prime factor for recently observed tropical oxygen trends [*Stramma et al*., 2008, 2012]. This is consistent with the work of *Monteiro et al*. [2011] who combined observational data and a simple conceptual model, to show that the regional ocean circulation drives the variability of hypoxia over the shelf. Our results reported here indicate the potential of high-resolution ocean general circulation models to unravel the linkages between global transport patterns and local biogeochemical environments.

Acknowledgments

This work is a contribution of the SFB754 supported by the Deutsche Forschungsgemeinschaft. The model system has been developed as part of the DRAKKAR collaboration. The simulations were performed at the North-German Supercomputing Alliance (HLRN) and the computing center at Kiel University. We thank Iris Kriest for sharing the biogeochemical model code. We thank Bill Johns for sharing the data of the mean velocity profile at 0°N/0°E, obtained from a mooring maintained by the University of Miami, as part of the CLIVAR TACE. Comments by Paul Kähler are appreciated.

The Editor thanks two anonymous reviewers for their assistance in evaluating this paper.

References

Behrenfeld, M. J., and P. G. Falkowski (1997), A consumer's guide to phytoplankton primary productivity models, *Limnol. Oceanogr.*, *42*(1), 1–20.

Bianchi, D., E. D. Galbraith, D. Carozza, K. A. S. Mislan, and C. Stock (2013), Intensification of open-ocean oxygen depletion by vertically migrating animals, *Nat. Geosci.*, *6*, 545–548, doi:10.1038/ngeo1837.

Brandt, P., V. Hormann, A. Koertzinger, M. Visbeck, G. Krahmann, L. Stramma, R. Lumpkin, and C. Schmidt (2010), Changes in the ventilation of the oxygen minimum zone of the tropical North Atlantic, *J. Phys. Oceanogr.*, *40*(8), 1784–1801.

Brandt, P., R. J. Greatbatch, M. Claus, S.-H. Didwischus, V. Hormann, A. Funk, J. Hahn, G. Krahmann, J. Fischer, and A. Koertzinger (2012), Ventilation of the equatorial Atlantic by the equatorial deep jets, *J. Geophys. Res.*, *117*, C12015, doi:10.1029/2012JC008118.

Cocco, V. F., et al. (2013), Oxygen and indicators of stress for marine life in multi-model global warming projections, *Biogeosciences*, *10*, 1849–1868, doi:10.5194/bg-10-1849-2013.

Debreu, L., C. Vouland, and E. Blayo (2008), AGRIF: Adaptive grid refinement in Fortran, *Comp. Geosci.*, *34*(1), 8–13.

Deutsch, C., H. Brix, T. Ito, H. Frenzel, and L. Thompson (2011), Climate-forced variability of ocean hypoxia, *Science*, *333*(6040), 336–339.

Dietze, H., and U. Loeptien (2013), Revisiting "nutrient trapping" in global biogeochemical ocean circulation models, *Global Biogeochem. Cycle*, *27*, 265–284, doi:10.1002/gbc.20029.

Duteil, O., and A. Oschlies (2011), Sensitivity of simulated extent and future evolution of marine suboxia to mixing intensity, *Geophys. Res. Lett.*, *38*, L06607, doi:10.1029/2011GL046877.

Duteil, O., et al. (2012), Preformed and regenerated phosphate in ocean general circulation models: Can right total concentrations be wrong?, *Biogeosciences*, *9*, 1797–1807, doi:10.5194/bg-9-1797-2012.

Garcia, H. E., R. A. Locarnini, T. P. Boyer, J. I. Antonov, O. K. Baranova, M. M. Zweng, and D. R. Johnson (2010), *World Ocean Atlas 2009*, Dissolved Oxygen, Apparent Oxygen Utilization, and Oxygen Saturation, vol. 3, edited by S. Levitus, 344 pp. NOAA Atlas NESDIS 70, U.S. Government Printing Office, Washington, D. C.

Gent, P. R., and J. C. McWilliams (1990), Isopycnal mixing in ocean circulation models, *J. Phys. Oceanogr.*, *20*, 150–155.

Getzlaff, J., and H. Dietze (2013), Effects of increased isopycnal diffusivity mimicking the unresolved equatorial intermediate current system in an earth system climate model, *Geophys. Res. Lett.*, *40*, 2166–2170, doi:10.1002/grl.50419.
Gnanadesikan, A., J. P. Dunne, and J. John (2012), Understanding why the volume of suboxic waters does not increase over centuries of global warming in an Earth System Model, *Biogeosciences*, *9*, 1159–1172, doi:10.5194/bg-9-1159-2012.
Goes, M., G. J. Goni, V. Hormann, and R. C. Perez (2013), Variability of eastward currents in the equatorial Atlantic during 1993–2010, *J. Geophys. Res. Oceans*, *118*, 3026–3045, doi:10.1002/jgrc.20186.
Johns, W. E., P. Brandt, B. Bourles, A. Tantet, and T. Papapostolou (2012), Zonal structure and variability of the Equatorial Undercurrent during TACE. TAV/PIRATA17 meeting, Kiel, Germany, September 2012.
Jouanno, J., F. Marin, Y. du Penhoat, J. M. Molines, and J. Sheinbaum (2011), Seasonal modes of surface cooling in the Gulf of Guinea, *J. Phys. Oceanogr.*, *41*, 1408–1416.
Kriest, I., S. Khatiwala, and A. Oschlies (2010), Towards an assessment of simple global marine biogeochemical models of different complexity, *Prog. Oceanogr.*, *86*(3–4), 337–360, doi:10.1016/j.pocean.2010.05.002.
Kriest, I., A. Oschlies, and S. Khatiwala (2012), Sensitivity analysis of simple global marine biogeochemical models, *Global Biogeochem. Cycle*, *26*, GB2029, doi:10.1029/2011GB004072.
Large, W. G., and S. G. Yeager (2009), The global climatology of an interannually varying air-sea flux data set, *Clim. Dyn.*, *33*, 341–364.
Luyten, J. R., J. Pedlosky, and H. Stommel (1983), The ventilated thermocline, *J. Phys. Oceanogr.*, *13*, 292–309.
Madec, G. (2008), NEMO ocean engine version 3.1. Note Pole Modelisation. 27, Inst. Pierre-Simon Laplace, Paris.
Martiny, A. C., C. T. A. Pham, F. Primeau, J. A. Vrugt, J. K. Moore, S. A. Levin, and M. W. Lomas (2013), Strong latitudinal patterns in the elemental ratios of marine plankton and organic matter, *Nat. Geosci.*, *6*, 279–283, doi:10.1038/ngeo1757.
Monteiro, P. M. S., B. Dewitte, M. I. Scranton, A. Paulmier, and A. K. Van der Plas (2011), The role of open ocean boundary forcing on seasonal to decadal-scale variability and long-term change of natural shelf hypoxia, *Environ. Res. Lett.*, *6*, 025002.
Moore, C. M., et al. (2013), Processes and patterns of oceanic nutrient limitation, *Nat. Geosci.*, *6*, 701–710, doi:10.1038/ngeo1765.
Najjar, R., et al. (2007), Impact of circulation on export production, dissolved organic matter, and dissolved oxygen in the ocean: Results from phase II of the Ocean Carbon-cycle Model Intercomparison Project (OCMIP-2), *Global Biogeochem. Cycle*, *21*, GB3007, doi:10.1029/2006GB002857.
Oschlies, A., K. G. Schultz, U. Riebesell, and A. Schmittner (2008), Simulated 21st century increase in oceanic suboxia by CO2-enhanced biotic carbon export, *Global Biogeochem. Cycle*, *22*, GB4008, doi:10.1029/2007GB003147.
Schmittner, A., A. Oschlies, X. Giraud, M. Eby, and H. L. Simmons (2005), A global model of the marine ecosystem for long term simulations: Sensitivity to ocean mixing, buoyancy forcing, particle sinking and dissolved organic matter cycling, *Global Biogeochem. Cycle*, *19*, GB3004, doi:10.1029/2004GB002283.
Stramma, L., and F. Schott (1999), The mean flow field of the tropical Atlantic Ocean, *Deep Sea Res., Part II*, *46*, 279–304, doi:10.1016/S0967-0645(98)00109-X.
Stramma, L., G. C. Johnson, J. Sprintall, and V. Mohrholz (2008), Expanding oxygen-minimum zones in the tropical oceans, *Science*, *320*, 655–658.
Stramma, L., A. Oschlies, and S. Schmidtko (2012), Mismatch between observed and modeled trends in dissolved upper-ocean oxygen over the last 50 yr, *Biogeosciences*, *9*, 4045–4057, doi:10.5194/bg-9-4045-2012.